Original Article

LNCAROD was stabilized through N^6-methyladenosine methylation and exerted its anticancer effects in lung squamous cell carcinoma by inhibiting SIRT1 activity via CCAR2

Qihang Yan[1,2,3#], Wingshing Wong[1,2#], Jinsong Lei[1,3#], Dachuan Liang[1], Jie Yang[1], Li Gong[1], Rossana Berardi[4], Shuqin Dai[1], Junye Wang[1,2,3]

[1]State Key Laboratory of Oncology in South China, Guangdong Provincial Clinical Research Center for Cancer, Sun Yat-sen University Cancer Center, Guangzhou, China; [2]Guangdong Esophageal Cancer Institute, Guangzhou, China; [3]Department of Thoracic Surgery, Sun Yat-sen University Cancer Center, Guangzhou, China; [4]Clinica Oncologica, Università Politecnica delle Marche, Azienda Ospedaliero-Universitaria delle Marche, Ancona, Italy

Contributions: (I) Conception and design: Q Yan, S Dai, J Wang; (II) Administrative support: Q Yan, W Wong, J Lei; (III) Provision of study materials or patients: J Wang; (IV) Collection and assembly of data: J Lei, D Liang, J Yang; (V) Data analysis and interpretation: Q Yan, W Wong; (VI) Manuscript writing: All authors; (VII) Final approval of manuscript: All authors.

[#]These authors contributed equally to this work.

Correspondence to: Junye Wang, MD. State Key Laboratory of Oncology in South China, Guangdong Provincial Clinical Research Center for Cancer, Sun Yat-sen University Cancer Center, 651 Dongfeng East Road, Guangzhou 510060, China; Guangdong Esophageal Cancer Institute, Guangzhou 510060, China; Department of Thoracic Surgery, Sun Yat-sen University Cancer Center, Guangzhou 510060, China. Email: wangjy@sysucc.org.cn; Shuqin Dai, MD. State Key Laboratory of Oncology in South China, Guangdong Provincial Clinical Research Center for Cancer, Sun Yat-sen University Cancer Center, 651 Dongfeng East Road, Guangzhou 510060, China. Email: daishq@sysucc.org.cn.

Background: Lung squamous cell carcinoma (LUSC), a deadly malignant tumor, is highly prevalent worldwide. Accumulating evidence indicates that long-chain noncoding RNAs play crucial regulatory roles in the occurrence and progression of LUSC. *LNCAROD* regulates the proliferation, migration, and invasion of cells by upregulating SERPINE1 expression in lung adenocarcinoma (LUAD). However, the functional mechanism of *LNCAROD* action in LUSC remains unclear. The aim of this study was to investigate the regulatory function and mechanism of *LNCAROD* action in the development of LUSC.

Methods: Using quantitative polymerase chain reaction (qPCR) detection, we determined the expression of *LNCAROD* in LUSC tissues and cell lines. Cell Counting Kit-8 (CCK-8), EdU (5-ethynyl-2'-deoxyuridine), JC-1 mitochondrial membrane potential, flow cytometry, colony formation, scratch healing, and Transwell assays were conducted, and cell proliferation, migration, and invasion, as well as physiological changes were assessed. The tumorigenicity of LUSC cells was analyzed by in vitro tumor formation in nude mice. Molecular interactions were verified via Western blotting, RNA-protein pull-down assay, RNA binding protein immunoprecipitation (RIP), N6-methyladenosine (m6A)-RIP, and coimmunoprecipitation (Co-IP) analyses.

Results: *LNCAROD* was specifically and highly expressed in LUSC cells and tissues. *LNCAROD* expression was mediated by IGF2BP2 m6A methylation, which, along with CCAR2, inhibited SIRTI1's acetylation activity. This further induced p53 protein acetylation and promoted the mitochondrial apoptosis of LUSC cells, thereby inhibiting cell proliferation, migration, and invasion.

Conclusions: *LNCAROD* is specifically highly expressed in LUSC cells and tissues and may be a tumor-suppressor gene. The findings contribute to a deeper understanding of the function of *LNCAROD* in LUSC, and it may serve as a potential prognostic marker for personalized medical diagnosis in clinical practice.

Keywords: *LNCAROD*; lung squamous cell carcinoma (LUSC); CCAR2; m6A methylation; SIRTI1

Submitted Mar 06, 2025. Accepted for publication Apr 23, 2025. Published online Apr 27, 2025.
doi: 10.21037/tlcr-2025-267
View this article at: https://dx.doi.org/10.21037/tlcr-2025-267

Introduction

Lung cancer is a malignant tumor with high global morbidity and mortality worldwide (1), with its incidence ranking second only to breast cancer. Lung squamous cell carcinoma (LUSC) accounts for nearly 30% of all histological lung cancer types (2), making it a key pathological subtype. As most cases of LUSC have no clear driver gene, chemotherapy is indispensable in the treatment of patients with nonsurgical advanced LUSC, with tyrosine kinase inhibitor (TKI) drug-targeted therapy being commonly applied in clinical settings (3). However, the etiology and mechanism of resistance to chemotherapy in LUSC remain unclear. Therefore, facilitating a greater understanding of the occurrence and development of LUSC and the changes underlying genetic and epigenetic mechanisms following chemotherapy is necessary for the development of more effective therapeutic interventional drugs. LUSC is a common pathological type of non-small cell lung cancer (NSCLC) (4), but at present, compared to lung adenocarcinoma (LUAD), research on its pathogenesis and treatment progress is lacking.

Long noncoding RNA (lncRNA) constitute a family of RNA with transcripts longer than 200 nucleotides and generally do not have a protein-coding function (5). LncRNAs are involved in epigenetic, transcriptional, and posttranscriptional regulation of gene expression in cells (6) and also participate in several biological processes, including cell growth, differentiation, and apoptosis (7). The expression of lncRNA *Hoxa-AS3* in NSCLC is upregulated following cisplatin treatment and its knockdown can enhance the efficacy of cisplatin *in vitro* and *in vivo*, thereby reducing the tolerance of cells to cisplatin. In one mechanism study, lncRNA *Hoxa-AS3* induced epithelial-mesenchymal transition (EMT) by downregulating the expression of HOXA3 to promote the cisplatin resistance of NSCLC cells (8). In breast cancer, lncRNA *SNHG1* promotes macrophage polarization toward the M2 phenotype and tumor growth and angiogenesis by regulating the phosphorylation of STAT6 (9). lncRNA *FGD5-AS1* is highly expressed in multiple cancers, and *FGD5-AS1* mediates the expression of *miR-520a-3p* and *KIAA1522* as a competing endogenous (ceRNA). Following the upregulation of KIAA1522 expression, KIAA1522 promotes the proliferation and migration of multiple cancers (10).

In eukaryotes, N6-methyladenosine (m6A) is the most abundantly occurring-and most studied and well-defined-mRNA methylation modification (11). *LncRNA-CBSLR* can interact with YTHDF2, resulting in the activation of the *CBSLR*/YTHDF2/CBS signaling axis in gastric cancer (12). Moreover, it decreases the stability of *CBS* messenger RNA (mRNA) through promoting the binding of YTHDF2 to the m6A-modified coding sequence (CDS) of *CBS* mRNA. Upregulation of CBSLR expression results in chemoresistance both *in vitro* and *in vivo* and is positively correlated with poor prognosis and poor chemotherapy efficacy. In gastric cancer, the expression of lncRNA *TP53TG1* is downregulated. ALKBH5 mediates the m6A modification of *TP53TG1*, thereby reducing the stability of ALKBH5 and downregulating its expression. This results in the weakening of the interaction between *TP53TG1* and CIP2A and the degradation of CIP2A via ubiquitination, which in turn contributes to the

Highlight box

Key findings

- To the best of our knowledge, this study is the first to demonstrate that *LNCAROD* is specifically and highly expressed in lung squamous cell carcinoma (LUSC) cells and tissues. Consistent with this, we found that *LNCAROD* expression was mediated by IGF2BP2 N6-methyladenosine methylation, which, along with CCAR2 inhibited, SIRTI1's acetylation activity. This leads to the inhibition of p53 protein acetylation, which eventually leads to mitochondrial apoptosis in LUSC cells, and the inhibition of cell proliferation, migration and invasion.

What is known and what is new?

- Long noncoding RNAs that regulate gene expression play a crucial role in tumorigenesis and progression.
- We found that *LNCAROD* could interact with CCAR2 through m6A methylation, inducing CCAR2 to suppress the activity of SIRT1, thereby enhancing the acetylation of the p53 protein.

What is the implication, and what should change now?

- The data presented in this study indicate that *LNCAROD* figures prominently in the onset and progression of LUSC. *LNCAROD* could serve as a future target for the development of novel therapeutic strategies.

occurrence and development of gastric cancer (13). In colorectal cancer (CRC), hypoxia induces HIF-1α, which mediates transcription and leads to the high expression of lncRNA *STEAP3-AS1*. *STEAP3-AS1* competitively binds to YTHDF2 and promotes the dissociation of *YTHDF2* and *STEAP3* mRNA. By protecting STEAP3 from m6A-mediated degradation, the upregulation of STEAP3 promotes the proliferation and metastasis of CRC *in vitro* and *in vivo* by upregulating Fe^{2+} and GSK3β phosphorylation and activating the WNT signaling pathway through β-catenin (14). The research on RNA m6A methylation is mainly centered on mRNA, and studies on lncRNA m6A methylation are scarce.

In this study, we identified a lncRNA, *LNCAROD*, which was found to be specifically expressed in LUSC and associated with poor overall survival and prognosis. In LUSC cells, *LNCAROD* could interact with CCAR2 through m6A methylation, facilitating CCAR2 in suppressing the activity of SIRT1, leading to enhanced acetylation of the p53 protein. *LNCAROD* could stabilize and maintain the activity of the CCAR2 protein to promote apoptosis and inhibit cell growth, migration, and invasion. We present this article in accordance with the ARRIVE and MDAR reporting checklists (available at https://tlcr.amegroups.com/article/view/10.21037/tlcr-2025-267/rc).

Methods

Gene set enrichment analysis (GSEA)

The goal of GSEA is to identify gene sets that are associated with particular biological processes or pathways (15). This is achieved by assessing the enrichment of the entire gene set across various biological conditions and by linking genes to predefined gene sets based on alterations in their expression levels. We obtained the h.all.v7.5.1.symbols from the Molecular Signature Database and used GSEA version 4.2.3 software to investigate the biological pathways related to the high or low expression of *LNCAROD*.

Tissue samples

All experiments involving human samples were reviewed and approved by the Ethics Committee of Sun Yat-sen University (approval No. SL-B2023-296-01). This study was conducted in accordance with the Declaration of Helsinki and its subsequent amendments. Tumor tissues and adjacent nontumor tissues were obtained from patients with LUSC (n=40) at Sun Yat-sen University Cancer Center. After surgical resection, samples were flash frozen in liquid nitrogen and stored in liquid nitrogen. No patient received any antineoplastic therapy before surgery. Preoperative candidates were informed about the study, with routine examinations performed 3 days before surgery. For this type of study, formal consent was not required, as many of the participants died when the study was initiated.

Cell lines

Human LUSC cell lines (SK-MES-1, NCI-H2170, NCI-H1703, and NCI-H520) and human normal lung epithelial cells (BEAS-2B) were purchased from Shanghai FuHeng Biology Co., Ltd. (Shanghai, China). SK-MES-1 cells were grown in minimal essential medium (MEM; Gibco, USA), and NCI-H2170, NCI-H1703, and NCI-H520 cells were grown in RPMI1640 medium (Gibco). BEAS-2B cells were grown in Dulbecco's Modified Eagle Medium (DMEM; Gibco). All media were supplemented with 10% fetal bovine serum (FBS; NEWZERUM, New Zealand) and penicillin and streptomycin (Gibco). All cells were cultured in a Heracell 150i CO_2 Incubator (Thermo Scientific, Waltham, MA, USA) at 37 ℃ in an environment with 5% CO_2.

Real-time quantitative polymerase chain reaction (RT-qPCR)

Total RNA was isolated from tissue samples and cells using the TRIzol reagent (Invitrogen, Thermo Fisher Scientific). After removal of trace amounts of genomic DNA from the total RNA sample with dsDNase, 1 μg of RNA was employed for reverse transcription in order to generate complement DNA (cDNA), with the Maxima First Strand cDNA Synthesis Kit (Thermo Fisher Scientific) used to conduct RT-qPCR. Reverse transcription was performed using a random primer for *LNCAROD* and *U6*. RT-qPCR was performed CFX96 (Bio-Rad Laboratories, USA), and the reaction system comprised the TB Green Fast qPCR Mix (Takara Bio, Japan). The quantification of changes in RNA expression was performed via the $2^{-\Delta\Delta Ct}$ method, with the primer sequences employed in this investigation detailed in *Table 1*.

Table 1 Primers used for qPCR

Name	Sequence
LNCAROD	F: CATGCTCCATCACATCATCCT
NR_120641.1	R: GCTCCAGCATGCAGAGATAA
LNCAROD	F: AGATGACAGAGTCTAGGTTAGGG
NR_120642.1	R: AGTAGCCTGTGTTCCTTCTAAAC
U6	F: GCTTCGGCAGCACATATACTA
NR_004394.1	R: CGAATTTGCGTGTCATCCTTG
GAPDH	F: CAAGAGCACAAGAGGAAGAGAG
NM_002046.7	R: CTACATGGCAACTGTGAGGAG
CCAR2	F: GATGATGGAGAGGAGGAGTTTG
NM_021174.6	R: GGCATGTCCTGAAGTGAAGA
IGF2BP2	F: AGCAGCAGGAGCAGAAATAC
NM_006548.6	R: GGTGTTGGAAGGGCTACATT

qPCR, quantitative polymerase chain reaction.

Table 2 The sequence of shRNA and siRNA

Name	Sequence
shRNA-NC	GTTGAGAGACCGTTGAGTAGA
LNCAROD-shRNA1	GCAGTGCAGGTTAATTCAATG
LNCAROD-shRNA2	GGCTACTGCGATGAGGATTGT
LNCAROD-shRNA3	GCCTGAGTCCTTGTAGACTCT
IGF2BP2-shRNA1	GGGTAAAGTGGAATTGCATGG
IGF2BP2-shRNA2	GCCGTTGTCAACGTCACATAT
IGF2BP2-shRNA3	GAACTACTCCTTCAAGATTTC
CCAR2-OE	NM_021174.6
CCAR2-shRNA1	GCGGGTCTTCACTGGTATTGT
CCAR2-shRNA2	GGTCTTCACTGGTATTGTTAC
CCAR2-shRNA3	GCCTCTGAGTCTCTTCCAAAC
AROS-OE	NM_194326.4
AROS-shRNA1	AGGCTGAGGGCACCGTGTTCA
AROS-shRNA2	GGCTGAGGGCACCGTGTTCAC
AROS-shRNA3	GCTGAGGGCACCGTGTTCACC
AROS-siRNA1	GGCACCGTGTTCACCGAGGAA
AROS-siRNA2	GCACCGTGTTCACCGAGGAAG
siRNA-NC	CTGCGTATGATGGCTCAGATTA

NC, negative control.

Construction of stable cell lines and transient gene expression

Overexpression plasmids and short hairpin (shRNA) constructs used in the study were purchased from GeneCopoeia (Rockville, USA). HEK293T cells were transfected using Hilymax reagent (Dojindo Laboratories, Kumamoto, Japan). Specifically, the target plasmid was cotransfected with helper packaging plasmids (psPAX2 and pMD2.G), and the cell supernatant was collected. After the lentivirus was obtained, SK-MES-1 and NCI-H1703 cells were transfected to establish stable gene-expressing cell lines. Small interfering RNA (siRNA) was synthesized by RiboBio Co., Ltd. (Guangzhou, China). Lipofectamin RNAiMAX (Invitrogen) was used for transfection. The gene sequence numbers, shRNA interference sequences, and siRNA sequences are listed in *Table 2*.

Cell viability assay

Cell viability was evaluated through via Cell Counting Kit-8 (CCK-8) Cell Proliferation and Cytotoxicity Assay Kit (Solarbio, China). Briefly, cells were seeded in 96-well plates at a density of 2,000 cells/well and were incubated for 12, 24, and 48 hours. Subsequently, 10 µL of CCK-8 solution was added per well, and cells were incubated for 1 hour at 37 ℃ in an environment with 5% CO_2. Absorbance was measured at 450 nm using the SpectraMax Plus 384 (Molecular Devices, USA).

EdU assay

The BeyoClic EdU Cell Proliferation Kit with Alexa Fluor 555 (Beyotime, China) was used. Cells were initially seeded onto poly-D-lysine (PDL)-coated cell slides at a density of approximately 60%. After treatment, the EdU working solution was introduced, and cells were subsequently incubated for 2 hours at 37 ℃ in an environment with 5% CO_2. Cells were fixed with 4% paraformaldehyde for a duration of 30 minutes and permeabilized for 15 minutes. Subsequently, the Click Additive Solution was administered, and the cells were incubated for an additional 30 minutes in darkness. Nuclei were labeled with 4',6-diamidino-2-phenylindole (DAPI). Observations were made using an ECLIPSE Ti-2 fluorescence microscope (Nikon, Japan) with Alexa Fluor 555 (Ex-555 nm and Em-565 nm) and Hoechst 33342 (Ex-346 nm and Em-460 nm).

Colony formation assay

For the colony formation assay, a total of 1,000 cells were initially plated in six-well cell culture plates and maintained at 37 ℃ in a 5% CO_2 environment for 10 days. The culture medium was refreshed every 3 days, and the cells were subsequently fixed with 4% paraformaldehyde (Beyotime) for 30 minutes, stained with crystal violet staining solution (Beyotime) for an additional 30 minutes, and rinsed with tap water. The quantification of cell colonies was conducted through manual enumeration, with each experimental condition being repeated three times.

Cell migration and invasion assays

Tumor cell migration and invasion were determined using 8 μm-pore Transwell inserts (Corning, USA). For invasion experiments, 15 μL of Matrigel (BD Biosciences, State of New Jersey, USA) was added to cells to simulate the internal environment of the tissue (16). Tumor cells were suspended in a serum-free medium and seeded in Transwell chambers at a density of 5×10^4–10×10^4 cells/0.2 mL. Transwell inserts were placed in the lower chamber containing 500 μL of complete medium, and cells were then incubated at 37 ℃ in a 5% CO_2 environment for a period ranging from 6 to 24 hours. Following this incubation, migrating or invading cells were fixed with 4% paraformaldehyde and subsequently stained with a 0.1% crystal violet solution. Observations were made using an ECLIPSE Ti-2 fluorescence microscope (Nikon, Japan).

Flow cytometry

Cell cycle analysis was performed using a cell cycle and apoptosis detection kit (Beyotime). Briefly, cells were digested with trypsin and harvested, incubated with 1 mL of prechilled 70% ethanol, and fixed at –20 ℃ overnight. After centrifugation, the cells were discarded from the supernatant, mixed with 0.5 mL of the propidium iodide (PI) staining solution (containing RNase A) was added, and then incubated for 30 minutes in the dark and at 37 ℃. Stained cells were analyzed using a CytoFLEX flow cytometer (Beckman Coulter, California, USA).

Cell line-derived xenograft

BALB/c female nude mice, aged 3–4 weeks, were purchased from GemPharmatech Co., Ltd. (Guangzhou, China). An equal number of SK-MES-1 cells were subcutaneously inoculated into nude mice. After 4 weeks, mice were killed and tumor tissues excised. Animal experiments were approved by the Ethics Committee of Sun Yat-sen University (approval No. L102012023060D), in compliance with Regulations for the administration of laboratory animals (2017) guidelines for the care and use of animals. A protocol was prepared before the study without registration.

Fluorescence in situ hybridization (FISH) assay

For FISH analysis of *LNCAROD*, the LINC01468 probe was synthesized by Ruibiotech (Guangzhou, China). Experiments were performed following the manufacturer's instructions, and cells were imaged using an FV1000 laser confocal microscope (Olympus, Japan).

Biotin RNA-protein pull-down assay and mass spectrometry analysis

The full-length *LNCAROD* RNA sequence was transcribed *in vitro* using the mMESSAGE mMACHINE Kit (Invitrogen, America). Specifically, 10× Biotin RNA labeling Mix (Roche) was used for *in vitro* biotin labeling of transcripts. Biotinylated transcripts were combined with total lysates from SK-MES-1 cells according to the manufacturer's instructions. Protein complexes bound to biotin RNA were enriched using streptavidin magnetic beads (Thermo Fisher Scientific). Mass spectrometry analysis was performed by Fitgene Co. Ltd. (Guangzhou, China).

Western blot analysis

Total intracellular protein was extracted using the RIPA buffer (Beyotime) containing protease inhibitors. Protein samples were quantified using a BCA protein concentration assay kit (Beyotime), subjected to separation via sodium dodecyl sulfate-polyacrylamide gel electrophoresis (SDS-PAGE) on 8–12% gels, and transferred onto polyvinylidene difluoride (PVDF) membranes (Merck, Darmstadt, Germany). Samples were treated with 5% skim milk and exposed to primary antibodies overnight at 4 ℃. Subsequently, after exposure to secondary antibodies, luminescence emitted by protein bands was identified with an ECL detection system (Thermo Fisher Scientific). The antibodies used for Western blot analysis are provided in *Table 3*.

Table 3 Antibodies used in WB

Name of antibody	Manufacturers	Article number
Anti-Bcl-2 antibody	Abcam	ab194583
Anti-cIAP1 antibody	Abcam	ab189193
Anti-Bax antibody	Abcam	ab32503
AIF Polyclonal antibody	Proteintech	17984-1-AP
Anti-ENDOGL1/ENGL antibody	Abcam	ab206300
Cytochrome c polyclonal antibody	Proteintech	10993-1-AP
Anti-p53 antibody	Abcam	ab32389
Anti-p53 (acetyl K120) antibody	Abcam	ab78316
Anti-p53 (acetyl K382) antibody	Abcam	ab75754
SIRT1 polyclonal antibody	Proteintech	13161-1-AP
Anti-DBC-1 (CCAR2) antibody	Abcam	ab215852
Anti-RPS19BP1/AROS antibody	Abcam	ab236598
Anti-Histone H3 antibody	Abcam	ab201456
Anti-GAPDH antibody	Abcam	ab181602
Goat anti-rabbit IgG HL (HRP)	Abcam	ab205718

WB, western blot.

Table 4 Antibodies used in RIP

Name of antibody	Manufacturers	Article number
Anti-DBC-1 (CCAR2) antibody	Abcam	ab215852
Anti-IGF2BP2/IMP-2 antibody	Abcam	ab128175
Rabbit anti-goat IgG HL	Abcam	ab6697
Anti-N6-methyladenosine (m6A) antibody	Abcam	ab151230

RIP, RNA Binding Protein Immunoprecipitation Assay.

RNA-binding protein immunoprecipitation

Total RNA was isolated from the cells the TRIzol reagent, which was followed by conjugation of target antibodies or anti-IgG antibodies with protein A/G magnetic beads and incubation with 100 μg of total RNA in an immunoprecipitation buffer containing RNase/protease inhibitors. The eluate was subjected to 2 rounds of elution for 1 hour each at 4 ℃. Subsequently, the resulting products were examined using RT-qPCR to ascertain the presence of protein-enriched RNA. The antibodies employed for the RNA-binding protein immunoprecipitation (RIP) analysis are detailed in *Table 4*.

Experimental drugs

Actinomycin D (ACTD) and cycloheximide (CHX) were purchased from Merck. MG132, Inauhzin, and SRT 1720 were purchased from Topscience Co. Ltd. (Shanghai, China).

Agarose gel electrophoresis

TAE buffer was used for the electrophoresis experiments. DNA was separated using 2% agarose gels, electrophoresed in TAE buffer, stained with the SerRed nucleic acid dye (Servicebio, China), and imaged on a Doc XR/ChemiDoc XRS+ Gel Imaging Analysis System (Bio-Rad Laboratories).

Analysis of subcellular segregation

Proteins of the cytoplasmic and nuclear fractions were isolated from cells using NEPER Nuclear and Cytoplasmic Extraction Reagents (Thermo Fisher Scientific). After the cells were lysed in the separation solution, nuclear and cytoplasmic fractions were separated by centrifugation. The expression of target proteins was detected by Western blot analysis, with GAPDH and H3 being used as cytoplasmic and nuclear controls, respectively.

Coimmunoprecipitation (Co-IP) analysis

Cells were harvested and lysed overnight via the addition of the RIPA lysis buffer containing phenylmethanesulfonyl fluoride (PMSF), phosphatase inhibitors, and protease inhibitors, along with 10% SDS and Triton X-100. A small amount of lysis buffer was used for Western blot analysis. After binding to the corresponding antibody, magnetic beads were subjected to binding with total proteins after cell lysis and incubated overnight at 4 ℃, with rotation being applied for coupling. After overnight incubation, magnetic beads were collected using a magnetic bar. The supernatant was carefully removed, and cells were washed 3–4 times with 1 mL of lysis buffer. Finally, 15 μL of 2× SDS loading buffer was added, and the specimens were boiled for 5 minutes. Western blotting was performed to analyze the abundance of the target proteins. Co-IP was performed using antibodies, as shown in *Table 5*.

Table 5 Antibodies used in Co-IP

Name of antibody	Manufacturers	Article number
Anti-DBC-1 (CCAR2) antibody	Abcam	ab215852
Anti-DDDDK tag (binding to the FLAG tag sequence) antibody	Abcam	ab205606

Co-IP, coimmunoprecipitation.

Table 6 Antibodies used in IF

Name of antibody	Manufacturers	Article number
Anti-p53 antibody	Abcam	ab32389
Goat anti-rabbit IgG HL (Alexa Fluor 488)	Abcam	ab150077

IF, immunofluorescence; IgG, immunoglobulin G.

RNA pulse-chase assay

The SK-MES-1 and NCI-H2170 cell lines were subjected to treatment with 5 μg/mL of Actinomycin D for specified durations. Subsequently, total cellular RNA was isolated using TRIzol reagent, which was followed by detection of RNA expression through RT-PCR.

CHX chase assay

SK-MES-1 cells were subjected to treatment with 50 μM of CHX, which was followed by the extraction of cellular proteins via RIPA lysis buffer containing protease inhibitors at specified time intervals. Protein expression was assessed through Western blot analysis.

JC-1 assay

Experiments were performed using the mitochondrial membrane potential assay kit with the JC-1 reagent (Beyotime, China). Cells were seeded in five-well plates, and experiments were performed following the specified protocol. Following removal of the supernatant, 1 mL of cell medium and 1 mL of the JC-1 staining working solution were added, and samples were incubated at 37 ℃ for 20 minutes in a 5% CO_2 environment. Samples were incubated with the JC-1 staining buffer and washed twice. Next, 2 mL of the cell culture medium was added and photographed using an ECLIPSE Ti-2 fluorescence microscope (Nikon) with JC-1 monomer (Ex-490 nm and Em-530 nm) and JC-1 polymer (Ex-525 nm and EM-590 nm).

Immunofluorescence assay

Cell slides were washed thrice with Dulbecco's Phosphate-Buffered Saline (DPBS) for 3 minutes each time. Subsequently, cells were fixed with 4% paraformaldehyde for 2 hours at 4 ℃. Sections were washed three times with PBS for 3 minutes each and incubated with 0.5% Triton X-100 at room temperature (25 ℃) for 20 minutes. The cells were washed three times with PBS for 3 minutes each time. Samples were incubated with goat serum at room temperature for 30 minutes for blocking. Primary antibodies were added to the sections and incubated overnight at 4 ℃. Samples were washed three times with Phosphate-Buffered Saline with Tween-20 (PBST) for 3 minutes each time. Fluorescent secondary antibodies were introduced to the cells, which were then incubated for 1 hour at room temperature. Subsequently, the cells were rinsed three times with PBST for 3 minutes each time, which was followed by quenching with a sealing solution containing DAPI anti-fluorescence quencher. The cells were then observed and photographed under a fluorescence microscope. Antibodies used for immunofluorescence (IF) staining analysis are listed in *Table 6*.

Statistical analysis

Experimental data are presented as the mean ± standard deviation (SD) of at least three independent experiments. The *t*-test or one-way analysis of variance (ANOVA) was used for comparison between and among multiple groups, respectively. Qualitative data were analyzed using the Chi-squared test. Kaplan-Meier analysis was used for survival analysis, and the log-rank test was used for comparisons between groups. Linear regression analysis was performed to assess the correlation between levels of gene expression. GraphPad Prism 8.0 (GraphPad Software, USA) and SPSS 27 (IBM Corp., USA) were used for statistical analysis. A P value less than 0.05 was considered statistically significant.

Results

LNCAROD was specifically expressed in LUSC and was associated with poor prognosis

Expression data were downloaded from the UCSC Xena database (https://xenabrowser.net/datapages/). Data were screened, and count data of lncRNAs were selected as the input for Differential Expression analysis of RNA-Seq data (DESeq2) for differential gene analysis. The results of the

differential analysis were input into Enhanced Volcano for displaying the volcano diagram (*Figure 1A*). The cellular localization of *LNCAROD* was identified. DESeq2 was used to analyze the differentially expressed lncRNAs between normal and tumor samples, of which 1,154 were upregulated and 325 were downregulated ($q<0.05$ and $|\log \text{fold change}| >2$). The heat map was plotted with ComplexHeatmap and showed the relative expression of the top 20 upregulated and downregulated genes (*Figure 1B*). Analysis of The Cancer Genome Atlas (TCGA) database showed that the expression of *LNCAROD* was significantly upregulated in LUSC tissues relative to the adjacent normal lung tissue (*Figure 1C*). In addition, 45 pairs of matched LUSCs and normal tissues also indicated significant upregulation of *LNCAROD* in tumors (*Figure 1D*). This conclusion was confirmed by RT-qPCR analysis of the clinical samples of LUSC and adjacent normal lung tissues (*Figure 1E*). Plotting the survival curve using a survival plot indicated that patients with LUSC with low *LNCAROD* expression had a worse overall prognosis (*Figure 1F*). To identify the potential function of lncRNA in LUSC, we performed GSEA and found that high expression of *LNCAROD* was closely related to cancer-related pathways such as EMT, cell junction, P53 pathway, angiogenesis, apoptosis, and hypoxia (*Figure 1G*). We selected *LNCAROD*, which is highly expressed in LUSC tissues and demonstrations clinical manifestations of tumor suppression, as our target. Specifically, through examination of the expression of two transcripts (NR_120641.1 and NR_120642.1) in human normal lung epithelial cells (BEAS-2B) and LUSC cells (SK-MES-1, NCI-H2170, NCI-H1703, and NCI-H520), only the transcript NR_120641.1 was found to be highly expressed in LUSC cells (*Figure 1H*). Compared with the human normal lung epithelial cell line, BEAS-2B, *LNCAROD*'s expression was upregulated in LUSC cell lines (SK-MES-1, NCI-H2170, NCI-H1703, and NCI-H520) (*Figure 1I*). The FISH probe for *LNCAROD* was used to determine its site of expression, and the results showed that *LNCAROD* expression was mainly localized to the nucleus (*Figure 1J*). In summary, *LNCAROD* was specifically expressed in LUSC and negatively correlated with the prognosis of patients with LUSC. Therefore, we inferred that *LNCAROD* inhibits tumorigenesis and development in LUSC.

LNCAROD inhibited the growth, migration, and invasion of LUSC cells

A cell line overexpressing *LNCAROD* (*LNCAROD*-OE) and that with shRNA interference (*LNCAROD*-shRNA) were obtained by lentivirus transfection, and the expression of *LNCAROD* was detected by RT-qPCR (*Figure 2A*). Stable *LNCAROD* overexpression and shRNA interference were successfully established in SK-MES-1 and NCI-H2170 cells. Among them, *LNCAROD*-shRNA1 showed the highest interference efficiency and was used for subsequent experimental studies. The CCK8 assay showed that the activities of SK-MES-1 and NCI-H2170 cells overexpressing *LNCAROD* were significantly downregulated, while those of SK-MES-1 and NCI-H2170 cells overexpressing *LNCAROD* were significantly upregulated (*Figure 2B*). EdU staining showed that the proliferation of SK-MES-1 and NCI-H2170 cells overexpressing *LNCAROD* was significantly suppressed, while that of SK-MES-1 and NCI-H2170 cells overexpressing *LNCAROD* was significantly enhanced (*Figure 2C*). Overexpression of *LNCAROD* slowed down the rate of cell clone formation, while interfering with *LNCAROD* expression promoted the formation of cell clones (*Figure 2D*). Overexpression of *LNCAROD* could inhibit the migration and invasion of LUSC cells, and interference with *LNCAROD* expression enhanced the migration and invasion of LUSC cells (*Figure 2E,2F*). Flow cytometry was performed for cell cycle analysis (*Figure 2G*). Overexpression of *LNCAROD* resulted in a slowing down of the cell cycle, decreased the cell proliferation rate, decreased the proportion of cells entering the S phase, and slowed cell division. Interfering with *LNCAROD* expression increased the cell proliferation rate, the proportion of cells entering the S phase, and the proportion of cells entering the G2 phase. In conclusion, *LNCAROD* could promote the proliferation and migration of LUSC cells, and its inhibition could promote cell proliferation, growth, migration, and metastasis. Thus, *LNCAROD* exerts a tumor suppressor effect in LUSC cells.

LNCAROD inhibited tumor formation in vivo

To verify the above-mentioned results, SK-MES-1 cells with *LNCAROD* were injected subcutaneously into nude mice (*Figure 3A*). After 28 days, tumors were excised, and those in the *LNCAROD*-OE group were significantly smaller than those in the control group, and tumors in the *LNCAORD*-shRNA group were significantly larger than those in the control group (*Figure 3B*). Growth curve analysis and final mass of the tumors in mice confirmed the above results (*Figure 3C,3D*). Xenograft tumor growth

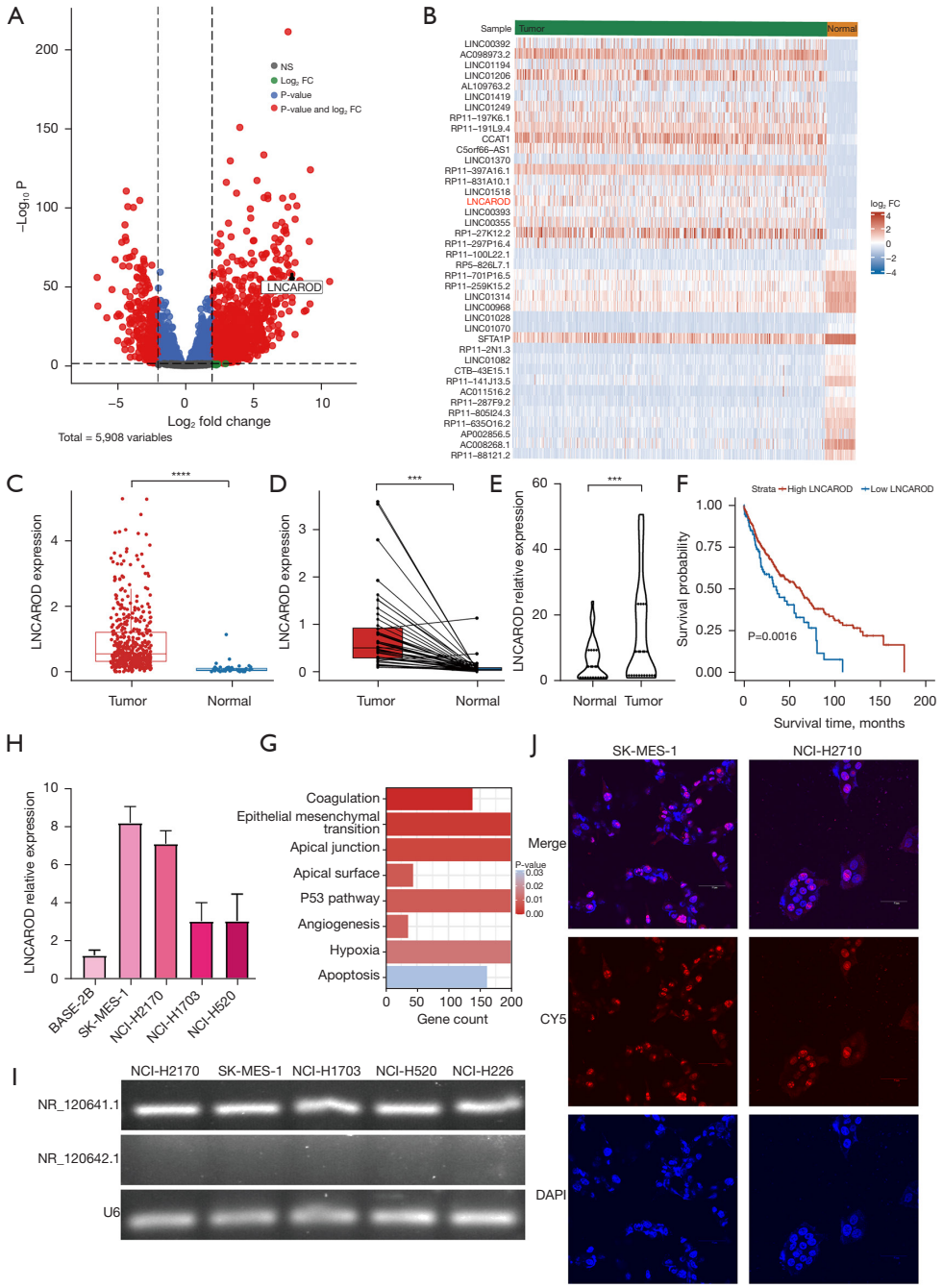

Figure 1 Expression of *LNCAROD* was upregulated in LUSC. (A) The volcano plot shows differentially expressed lncRNAs in LUSC. (B) The heatmap displays the lncRNA profile of lung cancer samples from TCGA. (C) TCGA database analysis of the expression status of *LNCAROD* in LUSC samples. (D) LUSC expression corresponded to LUSC expression in LUSC and normal tissues. (E) RT-qPCR was performed to detect the expression of *LNCAROD* in fresh LUSC and adjacent normal tissues. (F) Survival curves were plotted to analyze the relationship between the expression of *LNCAROD* and overall survival in patients with LUSC. (G) Enrichment analysis of the GSEA gene set. (H) RT-qPCR for the detection of transcripts of *LNCAROD* in LUSC cell lines and normal cells. (I) RT-qPCR was used to determine the expression of *LNCAROD* in LUSC cell lines. (J) FISH probes to detect the localization of *LNCAROD* (200×). ***, P<0.001; ****, P<0.0001; FC, fold change; GSEA, Gene Set Enrichment Analysis; LUSC, lung squamous cell carcinoma; TCGA, The Cancer Genome Atlas; RT-qPCR, real-time quantitative polymerase chain reaction; GSEA, gene set enrichment analysis; FISH, fluorescence in situ hybridization.

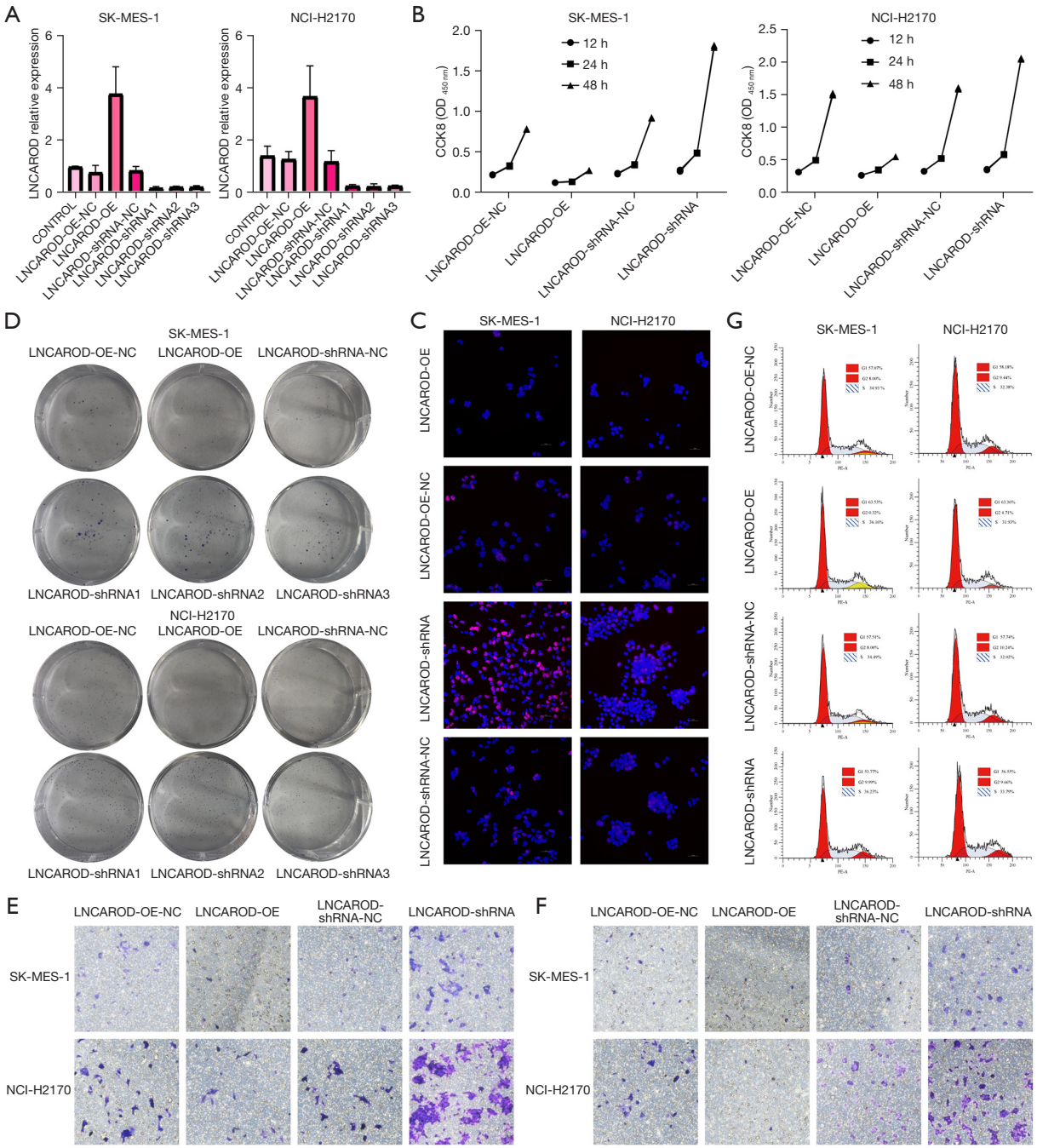

Figure 2 *LNCAROD* exerted inhibitory effects on the proliferation, migration, and invasion of LUSC cells. (A) Establishment of stable *LNCAROD*-overexpression and -knockdown cell lines. (B) CCK-8 assay was performed to analyze the effects of overexpression and knockdown of *LNCAROD* on cell proliferation. (C) EdU staining to assess the effect of overexpression and knockdown of *LNCAROD* on cell proliferation (200×). (D) Clonogenic and crystal violet staining assay to investigate the effect of overexpression and knockdown of *LNCAROD* on colony formation. (E) Transwell migration and crystal violet staining assay to evaluate the migratory ability of *LNCAROD*-overexpression or -knockdown LUSC cells (200×). (F) Transwell invasion and crystal violet staining assay to examine the invasive capacity of *LNCAROD*-overexpression or knockdown LUSC cells (200×). (G) Flow cytometry analysis to detect the effects of *LNCAROD* overexpression and knockdown on the cell cycle of LUSC cells. CCK-8, Cell Counting Kit-8; LUSC, lung squamous cell carcinoma; NC, negative control; OD, optical density; OE, overexpression.

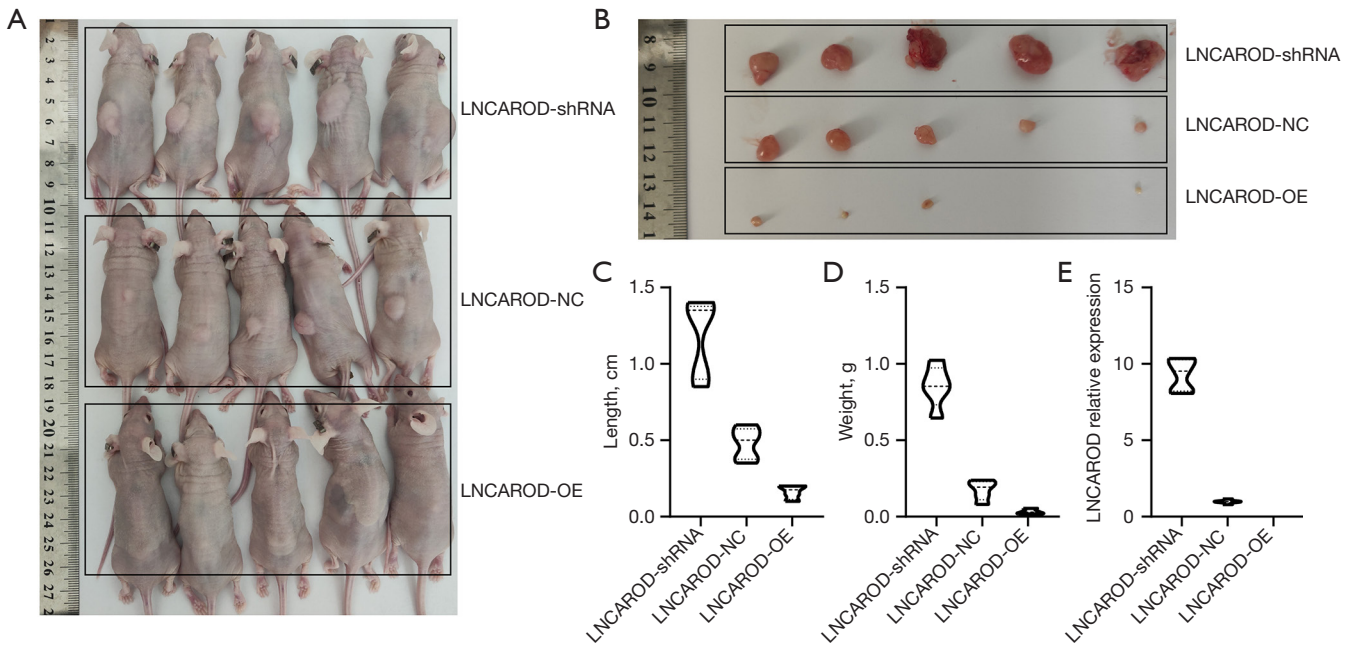

Figure 3 *LNCAROD* promoted tumor initiation *in vivo*. (A) Macroscopic view of nude mice with xenografted tumors. (B) Subcutaneous xenograft tumor body in nude mice. (C) Growth curves of xenografted tumors obtained from control, *LNCAROD*-overexpression, and *LNCAROD*-silenced SK-MES-1 cells. (D) Analysis of the weight of xenograft tumors. (E) qPCR detection of *LNCAROD* expression in tumors. NC, negative control; OE, overexpression; qPCR, quantitative polymerase chain reaction.

assay in nude mice showed inhibition of tumor growth in the *LNCAROD*-OE group, while *LNCAORD*-shRNA cells promoted tumor growth. The extraction of RNA from the tumor tissues for qPCR analysis revealed the expected expression of *LNCAROD* in the tumor, compared with the NC group, high expression occurred in the OE group and low expression occurred in the shRNA group (*Figure 3E*). These results indicated that a high expression of *LNCAORD* could inhibit the occurrence and development of LUSC tumors, and *LNCAROD* exerted a tumor-suppressing effect in LUSC.

IGF2BP2 regulated the stability of LNCAROD through m6A modification

Through our RNA pull-down and mass spectrometry experiments, IGF2BP2 was found to bind to *LNCAROD*. Since IGF2BP2 expression was associated with m6A methylation modification, we assessed whether IGF2BP2 mediated the m6A modification of *LNCAROD*. First, we examined the degree of IGF2BP2 enrichment in the pull-down assay of LNCAROD using Western blotting. IGF2BP2 was found to be bound to *LNCAROD* (*Figure 4A*). We performed RIP in SK-MES-1 and NCI-H2170 cells using anti-IGF2BP2, and the products were confirmed by qPCR analysis. *LNCAROD* was significantly enriched in the RIP product of anti-IGF2BP2 as compared to the IgG group, confirming the binding between IGF2BP2 and *LNCAROD* (*Figure 4B*). To verify whether *LNCAROD* was affected by m6A modification, we performed methylated (Me) RIP-qPCR assays. Knockdown of IGF2BP2 significantly reduced m6A modification of *LNCAROD* in SK-MES-1 and NCI-H2170 cells (*Figure 4C*). According to the sequence-based RNA adenosine methylation site predictor (SRAMP) software (http://www.cuilab.cn/sramp), six m6A sites were predicted in *LNCAROD* (*Figure 4D*). The mRNA stability assay showed that the knockdown of IGF2BP2 significantly downregulated *LNCAROD* expression and shortened the half-life of its RNA (*Figure 4E*). Overall, IGF2BP2 was associated with the m6A modification of *LNCAROD* and found to promote the stable expression of *LNCAROD*.

LNCAROD mediated the interaction between CCAR2 and AROS proteins

Based on these results, we explored the molecular

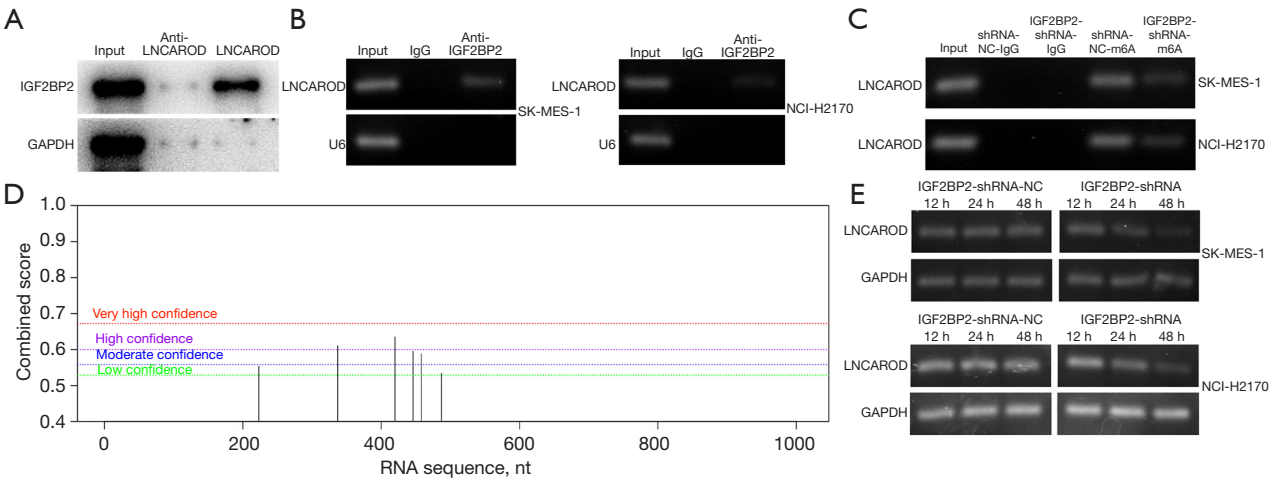

Figure 4 IGF2BP2 modulated the stability of *LNCAROD* through m6A modification. (A) RNA pull-down and Western blot analysis demonstrated the interaction between *LNCAROD* and IGF2BP2 proteins in SK-MES-1 cells. (B) RIP-qPCR analysis revealed the enrichment of *LNCAROD* in anti-IGF2BP2 precipitates. (C) MeRIP-qPCR experiments demonstrated an enhanced abundance of *LNCAROD* upon the silencing of IGF2BP2 in SK-MES-1 and NCI-H2170 cells. (D) SRAMP was used to predict m6A methylation sites on LNCARD. (E) Pulse-chase assays were conducted to assess the stability and expressional dynamics of *LNCAROD* in SK-MES-1 and NCI-H2170 cells following knockout of IGF2BP2 after treatment with actinomycin D (5 μg/mL) for an indicated duration. IgG, immunoglobulin G; NC, negative control; qPCR, quantitative polymerase chain reaction; RIP, RNA Binding Protein Immunoprecipitation Assay.

mechanism of *LNCAROD* as a tumor suppressor in the progression of LUSC. Proteins binding to *LNCAROD* in SK-MES-1 cells were identified by RNA pull-down and mass spectrometry. The combined results of the two showed that CCAR2 and AROS were bound to *LNCAROD*, which was verified at the protein level by Western blotting (*Figure 5A*). The results of the RIP assay showed that *LNCAROD* was precipitated by anti-CCAR2 in SK-MES-1 cells and NCI-H2170 cells (*Figure 5B*). The cytoplasmic and nuclear fractions of SK-MES-1 and NCI-H2170 cells were isolated by subcellular fractionation, and Western blotting showed that both CCAR2 and AROS proteins were localized in the nucleus (*Figure 5C*). Analysis of the deletion mutants showed that LNCAROD was bound to CCAR2 in the 1–250 nt region and AROS in the 251–500 nt region (*Figure 5D,5E*). We confirmed that exogenous and endogenous CCAR2 proteins immunoprecipitated with AROS proteins in SK-MES-1 cells (*Figure 5F*). Treatment of cell lysates with RNase A significantly reduced the association between CCAR2 and AROS as compared with treatment with RNase inhibitors, indicating the involvement of RNA in facilitating the association between CCAR2 and AROS (*Figure 5G*). Moreover, interfering with *LNCAROD* expression in SK-MES-1 cells suppressed the interaction between CCAR2 and AROS, which was enhanced by the overexpression of *LNCAROD* (*Figure 5H*). Silencing and overexpression of CCAR2 or AROS had little effect on *LNCAROD* expression in SK-MES-1 cells (*Figure 5I,5J*). However, overexpression of *LNCAROD* promoted CCAR2 expression, and its knockdown inhibited CCAR2 expression. Yet, *LNCAROD* expression did not affect AROS expression (*Figure 5K*). Overexpression or knockdown of *LNCAROD* also did not affect the mRNA levels of *CCAR2* and *AROS* (*Figure 5L,5M*). *LNCAROD* was associated with the half-life of CCAR2. Specifically, overexpression of *LNCAROD* prolonged the half-life of CCAR2, whereas its knockdown shortened it (*Figure 5N*). The degradation of CCAR2 protein could partially be rescued by treatment of SK-MES-1 and NCI-H2170 with MG132 to knockout *LNCAROD* (*Figure 5O*). The loss of *LNCAROD* accelerated the degradation of the CCAR2 protein. Silencing AROS in SK-MES-1 and NCI-H2170 cells did not reduce the protein and mRNA levels of CCAR2 (*Figure 5P,5Q*). Therefore, our data confirmed that *LNCAROD* could stabilize the protein expression of CCAR2 and interact with AROS, but its function should be investigated further.

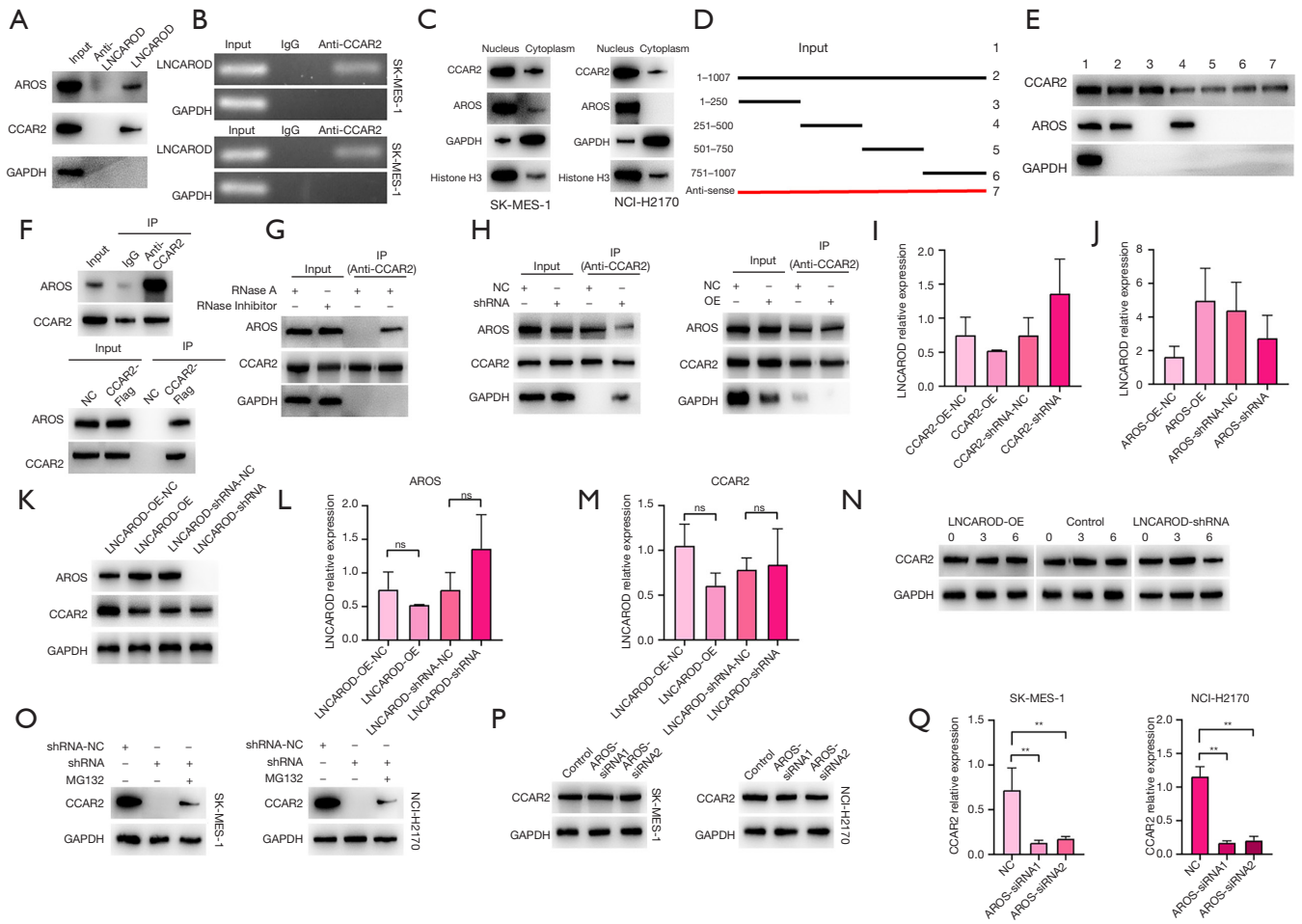

Figure 5 *LNCAROD* enhanced the stability of CCAR2 and facilitated the protein–protein interaction between CCAR2 and AROS. (A) RNA pull-down and Western blot analysis demonstrated the interaction between *LNCAROD*, CCAR2, and AROS proteins. (B) RIP-qPCR detection indicated the binding of CCAR2 to *LNCAROD*. (C) Subcellular fractionation and Western blot analysis showed localization of CCAR2 and AROS proteins in the nucleus of SK-MES-1 and NCI-H2170 cells. (D) Schematic representation depicting the full-length transcript of *LNCAROD* along with its deletion fragments. (E) The association between CCAR2, AROS proteins, and *LNCAROD* deletion fragments was confirmed through Western blot analysis. (F) Co-IP experiments indicated the coimmunoprecipitation of exogenous and endogenous AROS with CCAR2 in SK-MES-1 cells. (G) Co-IP experiments showed a weakened association between CCAR2 and AROS proteins in SK-MES-1 cells following treatment with RNase A. (H) Co-IP analysis indicated a correlation between CCAR2 and AROS proteins in SK-MES-1 cells transfected with *LNCAROD*-shRNA or *LNCAROD*-OE constructs. (I) Effects of silencing or overexpressing CCAR2 on the expression of *LNCAROD*. (J) Effects of silencing or overexpressing AROS on the expression of *LNCAROD*. (K) Effects of silencing or overexpressing *LNCAROD* on the protein expression of CCAR2. (L) Effect of silencing and overexpressing *LNCAROD* on AROS mRNA expression. (M) Effect of silencing and overexpressing *LNCAROD* on CCAR2 mRNA expression. (N) Cycloheximide chase analysis of CCAR2 protein levels in CHX-treated SK-MES-1 cells that silenced or overexpressed *LNCAROD*. (O) MG132 treatment prevented the decrease in CCAR2 protein levels in SK-MES-1 and NCI-H2170 after *LNCAROD* depletion. (P) Effect of AROS knockdown on CCAR2 protein expression. (Q) Effect of AROS knockdown on CCAR2 mRNA expression. **, P<0.01; ns, no significance. Co-IP, coimmunoprecipitation; NC, negative control; OE, overexpression; qPCR, quantitative polymerase chain reaction; RIP, RNA Binding Protein Immunoprecipitation Assay.

CCAR2 mediated the deacetylation of p53 by inhibiting the activation of SIRT1 by AROS

We experimentally investigated and explored whether the tumor-suppressive function of *LNCAROD* in LUSC cells is mediated by CCAR2. In SK-MES-1 and NCI-H2170 cells transfected with the *LNCAROD*-shRNA construct, re-expression of CCAR2 resulted in increased CCAR2 protein levels, increased p53 acetylation, and decreased SIRT1 protein expression. In LUSC cells transfected with *LNCAROD*-OE, interference of *CCAR2* expression resulted in the downregulation of the CCAR2 protein level and p53 acetylation, along with the upregulation of SIRT1 protein expression (*Figure 6A*). CHX chase assay showed that high *LNCAROD* expression enhanced p53 stability in LUSC cells, while interference of *LNCAROD* expression attenuated this stability. Knockdown of CCAR2 expression in *LNCAROD*-OE cells or overexpression of CCAR2 in *LNCAROD*-shRNA cells could compensate for this phenomenon (*Figure 6B*). IF analysis showed that overexpression of both *LNCAROD* and CCAR2 promoted the expression and cytoplasmic localization of acetylated p53, while interference with *LNCAROD* and CCAR2 resulted in the opposite (*Figure 6C*). In LUSC cells transfected with *LNCAROD*-OE constructs, overexpression of *AROS* or activation of SIRT1 promoted the downregulation of p53 acetylation and the upregulation of the SIRT1 protein expression. In LUSC cells transfected with *LNCAROD*-shRNA, interference with AROS expression or inhibition of SIRT1 activity resulted in the promotion of p53 acetylation and downregulation of SIRT1 protein expression (*Figure 6D*). CHX chase assay showed that overexpression of AROS or activation of SIRT1 promoted p53 degradation and inhibited the effect of *LNCAROD*-OE on p53 stability. Interference with AROS expression or inhibition of SIRT1 activity could enhance the stability of p53 and inhibit the reduced p53 protein stability due to the knockdown of *LNCAROD* (*Figure 6E*). IF staining showed that interference with AROS expression or inhibition of SIRT1 activity could promote the expression and cytoplasmic localization of acetylated p53, while overexpression of *AROS* or activation of SIRT1 resulted in the opposite (*Figure 6F*). These data suggest that CCAR2 mediates the effects of AROS and SIRT1 on p53 signaling.

LNCAROD stabilized the expression of CCAR2 and inhibits the proliferation, migration, and invasion of LUSC cells

Functionally, knockdown of *CCAR2* in LUSC cells transfected with the *LNCAROD*-OE construct rescued LUSC cells from reduced cell viability (*Figure 7A*), colony formation (*Figure 7B*), and cell proliferation (*Figure 7C*) and cell cycle arrest (*Figure 7D*). In contrast, overexpression of *CCAR2* in *LNCAROD*-shRNA-transfected LUSC cells rescued the tumor-promoting effect. Similar results were observed for cell migration and invasion (*Figure 7E*,*7F*). Knockdown of *CCAR2* rescued reduced cell migration and invasion in *LNCAROD*-OE-transfected LUSC cells. Overexpression of *CCAR2* rescued the upregulation of cell migration and invasion in *LNCAROD*-shRNA-transfected LUSC cells. Western blot analysis revealed that overexpression of *LNCAROD* (*Figure 7G*) resulted in the upregulation of BAX, AIF, ENDOG, and cytochrome C in the cells, concomitant with the downregulation of BCL-2 and c-IAP1. This phenomenon was enhanced by the downregulation of *CCAR2*. Conversely, the knockdown of *LNCAROD* with shRNA led to an increase in BCL-2 and c-IAP1 expression, along with a decrease in the levels of BAX, AIF, ENDOG, and cytochrome C. This effect was augmented by the upregulation of *CCAR2*. JC-1 staining of mitochondria (*Figure 7H*) revealed a decrease in mitochondrial membrane potential in *LNCAROD*-OE cells, which was restored following the downregulation of *CCAR2* expression. In *LNCAROD*-shRNA-transfected cells, the mitochondrial membrane potential was slightly enhanced, while it did not change significantly when the expression of *CCAR2* was upregulated.

Discussion

In head-and-neck squamous cell carcinoma (HNSCC), m6A methylation is known to enhance the stability of *LNCAROD* and bind to YBX1 and HSPA1A proteins to preserve the activity of YBX1. Knockdown of *LNCAROD* reduces cell proliferation and tumorigenicity *in vivo*, while its overexpression results in enhanced effects (17). In LUAD, SIX5 enhances the expression of *LNCAROD*. *LNCAROD* enhances the stability of *SERPINE1* mRNA by recruiting SERBP1 and interacts with USP5, thus affecting

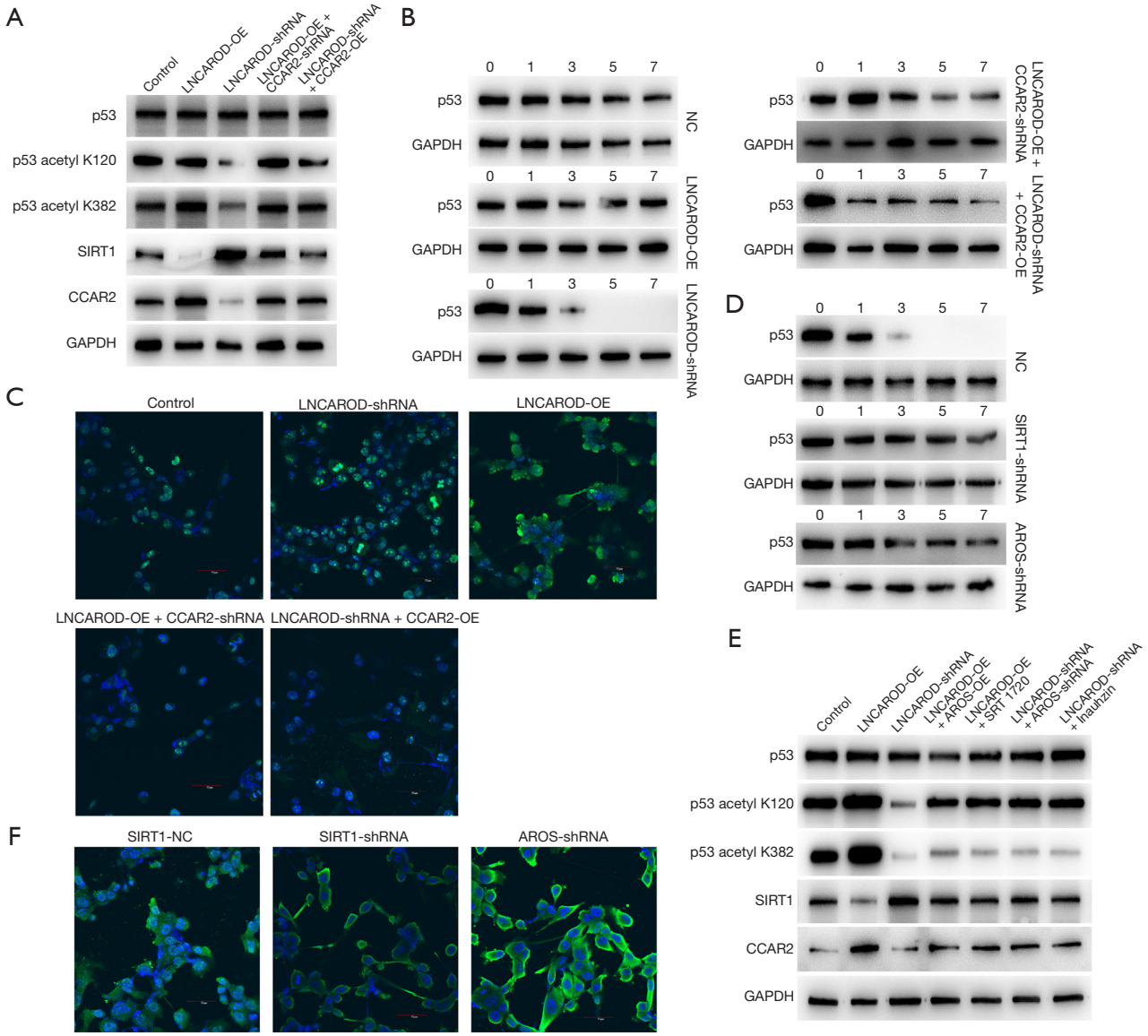

Figure 6 CCAR2 inhibited the activating effect of AROS on SIRT1 and suppressed the deacetylation of p53. (A) *LNCAROD* inhibited the deacetylation of p53 by CCAR2. (B) Cycloheximide chase analysis clarified the effect of *LNCAROD* and CCAR2 on the stability of p53 in SK-MES-1 cells. (C) Immunofluorescence staining confirmed the effect of *LNCAROD* and CCAR2 on the nuclear export of p53 in SK-MES-1 cells (200×). (D) Activation of SIRT1 or overexpression of AROS both facilitated p53 deacetylation. (E) Cycloheximide chase analysis demonstrated the effects of SIRT1 and AROS on p53 stability in SK-MES-1 cells. (F) Immunofluorescence staining confirmed the effect of SIRT1 and AROS on the nuclear export of p53 in SK-MES-1 cells (200×). NC, negative control; OE, overexpression.

the ubiquitination of PAI1 protein. The ubiquitination of PAI1 protein in turn promotes the proliferation, migration, and invasion of LUAD cells (18). *LNCAROD* acts as a conditional factor for enhancing the transcriptional activation of DKK through its nascent spliced released form (19). *LNCAROD* can enhance the transcription of DKK1 and increase its expression in MCF-7 breast cancer cells through a quasi-cis mechanism (20). As an inhibitor of the WNT signaling pathway, DKK1 is abnormally expressed in tumors, but its function remains controversial. A potential association between methylation of the DKK1 promoter and the development of early-stage tumors in NSCLC, as

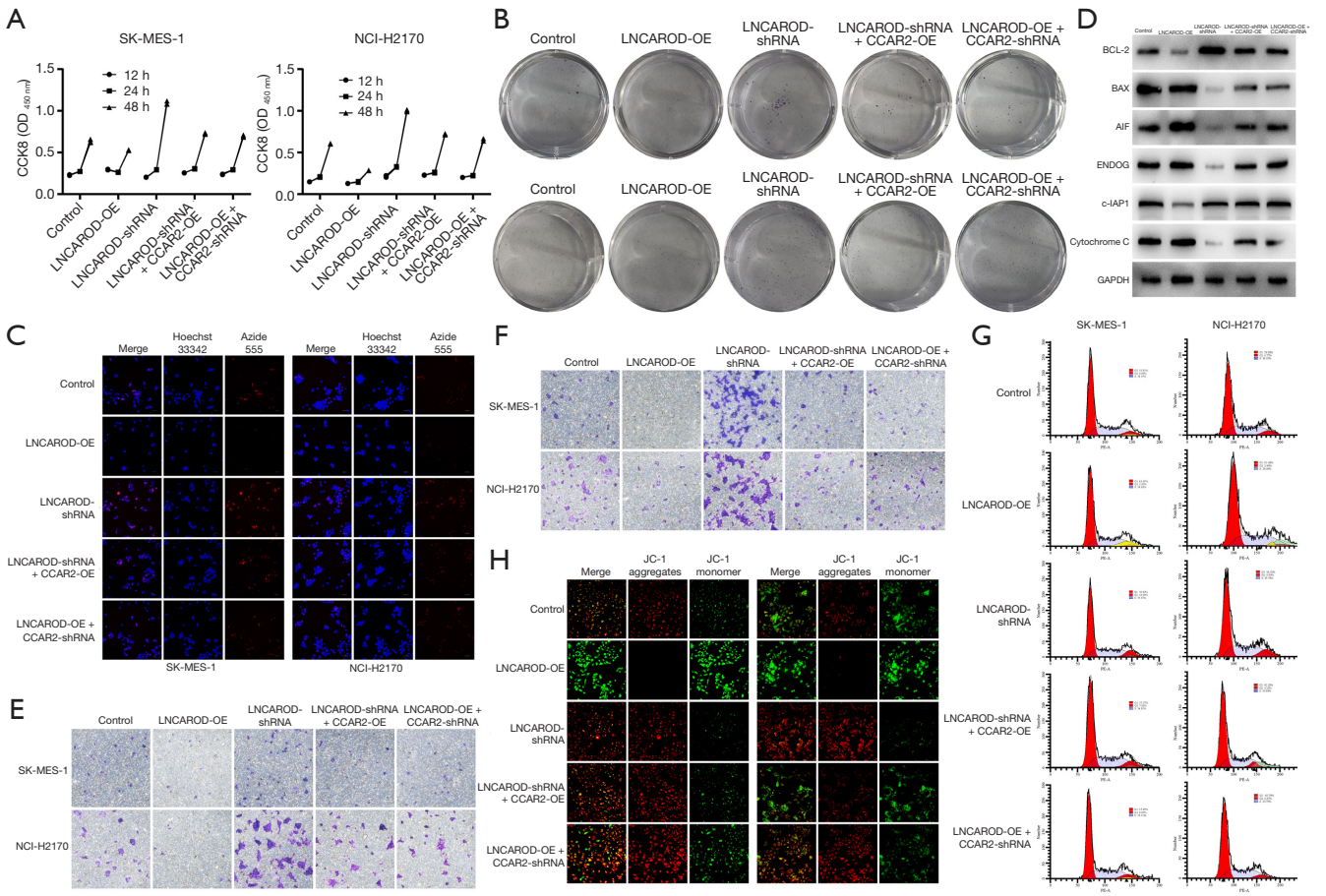

Figure 7 Overexpression of CCAR2 rescued the cellular phenotype of *LNCAROD* knockdown in *LNCAROD*-shRNA cells, while inhibition of CCAR2 expression rescued the cellular phenotype of overexpression of *LNCAROD* in *LNCAROD*-OE cells. (A) The effect of CCAR2 on the viability of SK-MES-1 and NCI-H2170 cells was assessed using CCK-8 assay. (B) The effect of CCAR2 on the proliferation of SK-MES-1 and NCI-H2170 cells was examined through colony formation and crystal violet staining assay. (C) The effect of CCAR2 on the proliferation of SK-MES-1 cells was evaluated using EdU staining (200×). (D) Western blotting for the detection of BCL-2, c-IAP1, BAX, AIF, ENDOG, and cytochrome C protein levels within the cells. (E) Transwell and crystal violet staining assay were conducted to assess the effect of CCAR2 on the migration of LUSC cells (200×). (F) Transwell and crystal violet staining assay were employed to determine the effect of CCAR2 on the invasion of LUSC cells (200×). (G) Flow cytometry analysis was performed to investigate the effect of CCAR2 on the cell cycle in LUSC cells. (H) Mitochondrial membrane potential in LUSC cells, and its alteration due to CCAR2, were detected via JC-1 staining (200×). CCK-8, Cell Counting Kit-8; LUSC, lung squamous cell carcinoma; OE, overexpression.

well as its effect on the prognosis of these patients, has been reported (21). In one study, Kaplan-Meier analysis of cancer stem cells (CSCs) and hepatocellular carcinoma (HCC) revealed that patients with low DKK1 expression exhibited significantly prolonged overall survival and cancer-specific survival compared to patients with high expression. Multivariate analysis further indicated a positive correlation between the mRNA expression of *DKK1* and cancer-specific survival rate (22). In our study, we identified *LNCAROD* as a tumor-suppressor gene involved in the pathogenesis and progression of LUSC. Specifically, in the context of LUSC, *LNCAROD* exerted its anticancer effects through CCAR2 to inhibit the deacetylation activity of SIRT1. This led to enhanced mitochondrial apoptosis in cells. Consequently, these molecular events resulted in a significant reduction in hallmarks of cancer cells, including proliferation, invasion, metastasis, and tumorigenicity, particularly in LUSC. Importantly, meticulous verification experiments conducted in this study unequivocally demonstrated that there is no discernible association between *LNCAROD* and previously

reported factors such as YBX1, HSPA1A, or PKM.

In the context of tumor cells, the functional role of CCAR2 remains debatable, and its potential as an oncogenic driver or tumor suppressor remains to be definitively elucidated. The interaction between CCAR2 and SIRT1 results in a negative regulation of SIRT1's function, thereby inhibiting its deacetylase activity (23). SIRT1 (24), an NAD^+-dependent deacetylase, can deacetylate both histone and nonhistone proteins. Moreover, SIRT1 deacetylates p53. In U2OS cells, Chk2 facilitates the interaction between CCAR2 and SIRT1, resulting in the suppression of SIRT1 deacetylase activity and the induction of apoptosis through the acetylation of p53. This phenomenon is not contingent upon Thr454 phosphorylation by CCAR2 (25). CCAR2 facilitates the expression of target genes of β-catenin, including PROX1, a transcription factor associated with the progression of CRC. Mechanistically, CCAR2 enhances the interactional stability of LEF1-β-catenin by inhibiting SIRT1-mediated deacetylation of β-catenin, leading to enhanced formation of the LEF1-β-catenin complex and long-range chromatin looping at PROX1 sites. CCAR2 exhibits dual functionality as a co-activator of β-catenin and PROX1 in regulating the β-catenin-PROX1 signaling axis, thereby maintaining the transcriptional activity of PROX1 (26). In the experimental context, LNCAROD expression was positively correlated with the activity of CCAR2, and LNCAROD inhibited the deacetylase activity of SIRT1 by stabilizing CCAR2 and activating CCAR2. The deacetylase activity of SIRT1 is inhibited, resulting in deacetylation inactivation of p53, which undergoes acetylation and is transferred from the nucleus to the outside, triggering the activation of apoptosis.

IGF2BP2 is an integral part of the m6A signaling pathway and plays a crucial role in tumor development. The IGF2BP protein, unlike the proteins of the YTH domain family, serves as an exceptional m6A reader by promoting mRNA stability rather than degradation. Unlike m6A readers containing YTH domains, IGF2BPs exert their effect on target RNAs (including MYC) through an m6A-dependent mechanism, thus enhancing both their stability and expression under normal and stress conditions. This is in contrast to the RNA decay-promoting function of YTH domain-containing family protein 2, which ultimately affects the intricate process of gene expression (27). In CRC cells (28), METTL3 functions as an oncogene and sustains the expression of SOX2 in an m6A-IGF2BP2-dependent manner. In CRC tissues, the expression of SOX2 and both METTL3 and IGF2BP2 are positively correlated. In HCC tissues (29), elevated levels of IGF2BP2 are associated with an unfavorable prognosis, while its overexpression can promote the proliferation of HCC cells *in vivo* and *in vitro*. This is attributed to the direct recognition and binding of IGF2BP to the m6A site on *FEN1* mRNA, which enhances its stability. Consequently, it is a promising biomarker for predicting the prognoses of patients with HCC. Our results show that LNCAROD stabilizes LNCAROD expression in LUSC by binding to IGF2BP2, and the mechanism is related to the occurrence of m6A in LNCAROD. Stable LNCAROD triggers the molecular mechanism by which CCAR2 in the nucleus inhibits sirt1 activity, leading to the inhibition of sirt1 deacetylation of p53, and finally triggering cell apoptosis based on the transfer of acetylated p53 from the nucleus to the outside of the nucleus.

The p53 protein plays a dual role in cellular growth, serving to maintain the stability of DNA and induction of apoptosis. One study reported that transfection of p53/MDM2-siRNA into SKOV3/DDP cells enhanced their sensitivity to cisplatin and effectively suppressed tumor cell proliferation both *in vitro* and *in vivo* (30). At low concentrations of H_2O_2, p53 stimulates the cellular production of antioxidant enzymes to counteract the toxicity due to reactive oxygen species (ROS). However, at high concentrations of H_2O_2, the activation of pro-oxidative genes is triggered within cells, indicating that p53 may function as a regulatory switch to induce expressions of distinct genes and elicit diverse stress responses. The transition between these two states is likely affected by the magnitude of the stress stimulus (31). p53 can trigger cell apoptosis in a transcription-independent manner devoid of transactivation of genes (32). Additionally, p53 can directly interact with mitochondria to enhance apoptotic activity (33) or act as a substitute for BH3 proteins. Upon being hindered from entering the nucleus by nuclear transfer inhibitors and forced to express in the cytoplasm, it can induce Bax activation (34). p53 also exhibits diverse cellular functions, with the specific role determined by the type and severity of cellular stress. In our study, despite the presence of an R280K mutation in p53 within SK-MES-1 cells (35), SIRT1-mediated deacetylation of p53R280K or p53 induced mitochondrial apoptosis was not impeded. These findings are promising for the development of future therapeutic interventions targeting p53-mutated LUSC.

Conclusions

The differential expression of *LNCAROD* was identified

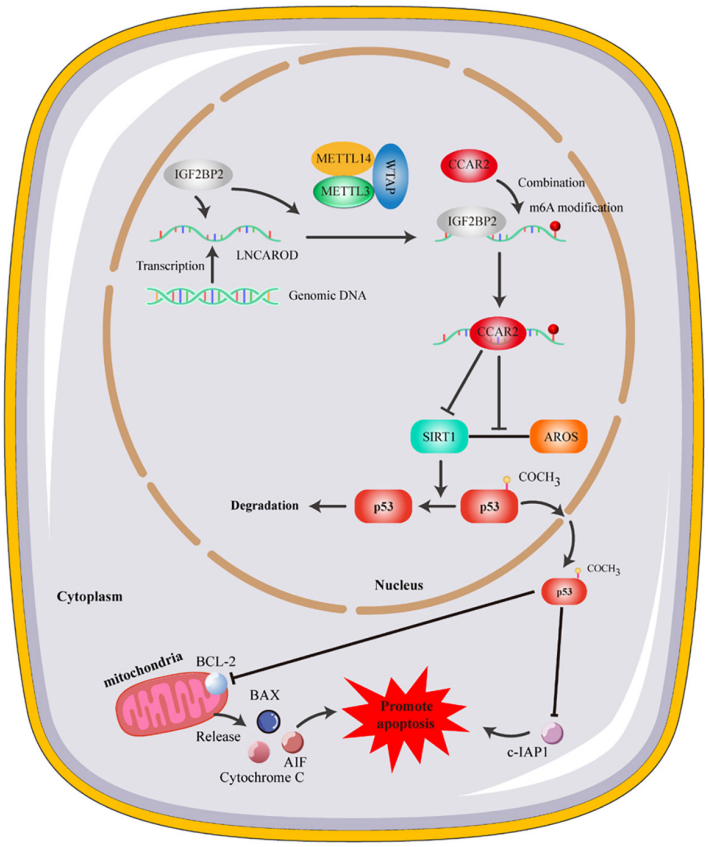

Figure 8 Schematic of the mechanism. *LNCAROD* hinders the activation of SIRT1 by facilitating the interaction between CCAR2 and AROS in LUSC cells, thereby suppressing p53 deacetylation. This leads to the acetylation and mitochondrial translocation of p53, thereby activating mitochondrial apoptosis and inducing tumor cell death. Thus, *LNCAROD* plays a role in suppressing cancer hallmarks in LUSC. LUSC, lung squamous cell carcinoma.

as a potential prognostic marker for LUSC. Furthermore, IGF2BP2-mediated m6A methylation was found to stabilize *LNCAROD* and facilitate CCAR2 in maintaining protein stability. This process inhibits AROS activation of SIRT1, ultimately regulating p53 acetylation and nuclear export to induce mitochondrial apoptosis, which, in turn, could mediate the occurrence and development of LUSC. Based on our findings, we identified *LNCAROD* as a promising diagnostic marker and endogenous tumor-suppressor gene in LUSC. The elucidation of a regulatory network involving *LNCAROD*/CCAR2/SIRT1/p53 (*Figure 8*) provides a more comprehensive means to investigating the pathogenesis and progression of LUSC, along with the associated mechanisms.

Acknowledgments

We are sincerely grateful to the staff of the Guangdong Esophageal Cancer Institute for their help in completing the project.

Footnote

Reporting Checklist: The authors have completed the ARRIVE and MDAR reporting checklists. Available at https://tlcr.amegroups.com/article/view/10.21037/tlcr-2025-267/rc

Data Sharing Statement: Available at https://tlcr.amegroups.com/article/view/10.21037/tlcr-2025-267/dss

Peer Review File: Available at https://tlcr.amegroups.com/article/view/10.21037/tlcr-2025-267/prf

Funding: This study was supported by the National Natural Science Foundation of China (No. 82173293) and the Natural Science Foundation of Guangdong Province (No. 2019A1515011601).

Conflicts of Interest: All authors have completed the ICMJE uniform disclosure form (available at https://tlcr.amegroups.com/article/view/10.21037/tlcr-2025-267/coif). R.B. reports that his institution receives funding from Astra Zeneca, Pfizer, and Roche, and that he serves on the Advisory Board of Bayer, Boeringher Ingelheim, EISAI, Lilly, Menarini, and GSK. The other authors have no conflicts of interest to declare.

Ethical Statement: The authors are accountable for all aspects of the work in ensuring that questions related to the accuracy or integrity of any part of the work are appropriately investigated and resolved. All experiments involving human samples were reviewed and approved by the Ethics Committee of Sun Yat-sen University (approval No. SL-B2023-296-01). This study was conducted in accordance with the Declaration of Helsinki and its subsequent amendments. For this type of study, formal consent was not required, as many of the participants died when the study was initiated. Animal experiments were approved by the Ethics Committee of Sun Yat-sen University (approval No. L102012023060D), in compliance with Regulations for the administration of laboratory animals (2017) guidelines for the care and use of animals.

References

1. Riely GJ, Wood DE, Ettinger DS, et al. Non-Small Cell Lung Cancer, Version 4.2024, NCCN Clinical Practice Guidelines in Oncology. J Natl Compr Canc Netw 2024;22:249-74.
2. Bray F, Laversanne M, Sung H, et al. Global cancer statistics 2022: GLOBOCAN estimates of incidence and mortality worldwide for 36 cancers in 185 countries. CA Cancer J Clin 2024;74:229-63.
3. Zhong H, Wang L, Zhu X, et al. STAT3 inhibitor Stattic Exhibits the Synergistic Effect with FGFRs Inhibitor Erdafitinib in FGFR1-positive Lung Squamous Cell Carcinoma. J Cancer 2024;15:5415-24.
4. Zhang S, Liu L, Shi S, et al. Bidirectional Association Between Cardiovascular Disease and Lung Cancer in a Prospective Cohort Study. J Thorac Oncol 2024;19:80-93.
5. Herbst RS, Morgensztern D, Boshoff C. The biology and management of non-small cell lung cancer. Nature 2018;553:446-54.
6. Huang W, Xiong T, Zhao Y, et al. Computational prediction and experimental validation identify functionally conserved lncRNAs from zebrafish to human. Nat Genet 2024;56:124-35.
7. Bridges MC, Daulagala AC, Kourtidis A. LNCcation: lncRNA localization and function. J Cell Biol 2021;220:e202009045.
8. Lin S, Zhang R, An X, et al. LncRNA HOXA-AS3 confers cisplatin resistance by interacting with HOXA3 in non-small-cell lung carcinoma cells. Oncogenesis 2019;8:60.
9. Zong S, Dai W, Guo X, et al. LncRNA-SNHG1 promotes macrophage M2-like polarization and contributes to breast cancer growth and metastasis. Aging (Albany NY) 2021;13:23169-81.
10. Lin J, Liao S, Liu Z, et al. LncRNA FGD5-AS1 accelerates cell proliferation in pancreatic cancer by regulating miR-520a-3p/KIAA1522 axis. Cancer Biol Ther 2021;22:257-66.
11. Qiu Y, Man C, Zhu L, et al. R-loops' m6A modification and its roles in cancers. Mol Cancer 2024;23:232.
12. Yang H, Hu Y, Weng M, et al. Hypoxia inducible lncRNA-CBSLR modulates ferroptosis through m6A-YTHDF2-dependent modulation of CBS in gastric cancer. J Adv Res 2022;37:91-106.
13. Fang D, Ou X, Sun K, et al. m6A modification-mediated lncRNA TP53TG1 inhibits gastric cancer progression by regulating CIP2A stability. Cancer Sci 2022;113:4135-50.
14. Zhou L, Jiang J, Huang Z, et al. Hypoxia-induced lncRNA STEAP3-AS1 activates Wnt/β-catenin signaling to promote colorectal cancer progression by preventing m(6)A-mediated degradation of STEAP3 mRNA. Mol Cancer 2022;21:168.
15. Subramanian A, Tamayo P, Mootha VK, et al. Gene set

enrichment analysis: a knowledge-based approach for interpreting genome-wide expression profiles. Proc Natl Acad Sci U S A 2005;102:15545-50.
16. Li J, Wang W, Chen S, et al. FOXA1 reprograms the TGF-β-stimulated transcriptional program from a metastasis promoter to a tumor suppressor in nasopharyngeal carcinoma. Cancer Lett 2019;442:1-14.
17. Ban Y, Tan P, Cai J, et al. LNCAROD is stabilized by m6A methylation and promotes cancer progression via forming a ternary complex with HSPA1A and YBX1 in head and neck squamous cell carcinoma. Mol Oncol 2020;14:1282-96.
18. Yuan Y, Zhou D, Chen F, et al. SIX5-activated LINC01468 promotes lung adenocarcinoma progression by recruiting SERBP1 to regulate SERPINE1 mRNA stability and recruiting USP5 to facilitate PAI1 protein deubiquitylation. Cell Death Dis 2022;13:312.
19. Ntini E, Louloupi A, Liz J, et al. Long ncRNA A-ROD activates its target gene DKK1 at its release from chromatin. Nat Commun 2018;9:1636.
20. Zhou XL, Qin XR, Zhang XD, et al. Downregulation of Dickkopf-1 is responsible for high proliferation of breast cancer cells via losing control of Wnt/beta-catenin signaling. Acta Pharmacol Sin 2010;31:202-10.
21. Stewart DJ. Wnt signaling pathway in non-small cell lung cancer. J Natl Cancer Inst 2014;106:djt356.
22. Suda T, Yamashita T, Sunagozaka H, et al. Dickkopf-1 Promotes Angiogenesis and is a Biomarker for Hepatic Stem Cell-like Hepatocellular Carcinoma. Int J Mol Sci 2022;23:2801.
23. Wang Y, Wang M, Chen J, et al. The gut microbiota reprograms intestinal lipid metabolism through long noncoding RNA Snhg9. Science 2023;381:851-7.
24. Jiang T, Liu E, Li Z, et al. SIRT1-Rab7 axis attenuates NLRP3 and STING activation through late endosomal-dependent mitophagy during sepsis-induced acute lung injury. Int J Surg 2024;110:2649-68.
25. Wagle S, Park SH, Kim KM, et al. DBC1/CCAR2 is involved in the stabilization of androgen receptor and the progression of osteosarcoma. Sci Rep 2015;5:13144.
26. Yu EJ, Kim SH, Kim HJ, et al. Positive regulation of β-catenin-PROX1 signaling axis by DBC1 in colon cancer progression. Oncogene 2016;35:3410-8.
27. Huang H, Weng H, Sun W, et al. Recognition of RNA N(6)-methyladenosine by IGF2BP proteins enhances mRNA stability and translation. Nat Cell Biol 2018;20:285-95.
28. Li T, Hu PS, Zuo Z, et al. METTL3 facilitates tumor progression via an m(6)A-IGF2BP2-dependent mechanism in colorectal carcinoma. Mol Cancer 2019;18:112.
29. Pu J, Wang J, Qin Z, et al. IGF2BP2 Promotes Liver Cancer Growth Through an m6A-FEN1-Dependent Mechanism. Front Oncol 2020;10:578816.
30. Gu J, Tang Y, Liu Y, et al. Murine double minute 2 siRNA and wild-type p53 gene therapy enhances sensitivity of the SKOV3/DDP ovarian cancer cell line to cisplatin chemotherapy in vitro and in vivo. Cancer Lett 2014;343:200-9.
31. Freire TS, Mori MP, Miranda JNFA, et al. Increased H2O2 levels and p53 stabilization lead to mitochondrial dysfunction in XPC-deficient cells. Carcinogenesis 2021;42:1380-9.
32. Liu Y, Su Z, Tavana O, et al. Understanding the complexity of p53 in a new era of tumor suppression. Cancer Cell 2024;42:946-67.
33. Zeng Y, He Y, Wang L, et al. Dihydroquercetin improves experimental acute liver failure by targeting ferroptosis and mitochondria-mediated apoptosis through the SIRT1/p53 axis. Phytomedicine 2024;128:155533.
34. Seo SU, Woo SM, Lee SG, et al. BAP1 phosphorylation-mediated Sp1 stabilization plays a critical role in cathepsin K inhibition-induced C-terminal p53-dependent Bax upregulation. Redox Biol 2022;53:102336.
35. Magrini R, Russo D, Fronza G, et al. The kinetics of p53-binding and histone acetylation at target promoters do not strictly correlate with gene expression after UV damage. J Cell Biochem 2007;100:1276-87.

(English Language Editor: J. Gray)

Cite this article as: Yan Q, Wong W, Lei J, Liang D, Yang J, Gong L, Berardi R, Dai S, Wang J. *LNCAROD* was stabilized through N^6-methyladenosine methylation and exerted its anticancer effects in lung squamous cell carcinoma by inhibiting SIRT1 activity via CCAR2. Transl Lung Cancer Res 2025;14(4):1351-1370. doi: 10.21037/tlcr-2025-267